

Deep Image Homography Estimation

Daniel DeTone
Magic Leap, Inc.
Mountain View, CA
ddetone@magicleap.com

Tomasz Malisiewicz
Magic Leap, Inc.
Mountain View, CA
tmalisiewicz@magicleap.com

Andrew Rabinovich
Magic Leap, Inc.
Mountain View, CA
arabinovich@magicleap.com

Abstract—We present a deep convolutional neural network for estimating the relative homography between a pair of images. Our feed-forward network has 10 layers, takes two stacked grayscale images as input, and produces an 8 degree of freedom homography which can be used to map the pixels from the first image to the second. We present two convolutional neural network architectures for HomographyNet: a regression network which directly estimates the real-valued homography parameters, and a classification network which produces a distribution over quantized homographies. We use a 4-point homography parameterization which maps the four corners from one image into the second image. Our networks are trained in an end-to-end fashion using warped MS-COCO images. Our approach works without the need for separate local feature detection and transformation estimation stages. Our deep models are compared to a traditional homography estimator based on ORB features and we highlight the scenarios where HomographyNet outperforms the traditional technique. We also describe a variety of applications powered by deep homography estimation, thus showcasing the flexibility of a deep learning approach.

I. INTRODUCTION

Sparse 2D feature points are the basis of most modern Structure from Motion and SLAM techniques [9]. These sparse 2D features are typically known as corners, and in all geometric computer vision tasks one must balance the errors in corner detection methods with geometric estimation errors. Even the simplest geometric methods, like estimating the homography between two images, rely on the error-prone corner-detection method.

Estimating a 2D homography (or projective transformation) from a pair of images is a fundamental task in computer vision. The homography is an essential part of monocular SLAM systems in scenarios such as:

- Rotation only movements
- Planar scenes
- Scenes in which objects are very far from the viewer

It is well-known that the transformation relating two images undergoing a rotation about the camera center is a homography, and it is not surprising that homographies are essential for creating panoramas [3]. To deal with planar and mostly-planar scenes, the popular SLAM algorithm ORB-SLAM [14] uses a combination of homography estimation and fundamental matrix estimation. Augmented Reality applications based on planar structures and homographies have been well-studied [16]. Camera calibration techniques using planar structures [20] also rely on homographies.

The traditional homography estimation pipeline is composed of two stages: corner estimation and robust homography estimation. Robustness is introduced into the corner detection stage by returning a large and over-complete set of points, while robustness into the homography estimation step shows up as heavy use of RANSAC or robustification of the squared loss function. Since corners are not as reliable as man-made linear structures, the research community has put considerable effort into adding line features [18] and more complicated geometries [8] into the feature detection step. What we really want is a single robust algorithm that, given a pair of images, simply returns the homography relating the pair. *Instead of manually engineering corner-ish features, line-ish features, etc, is it possible for the algorithm to learn its own set of primitives?* We want to go even further, and add the transformation estimation step as the last part of a deep learning pipeline, thus giving us the ability to learn the entire homography estimation pipeline in an end-to-end fashion.

Recent research in dense or direct featureless SLAM algorithms such as LSD-SLAM [6] indicates promise in using a full image for geometric computer vision tasks. Concurrently, deep convolutional networks are setting state-of-the-art benchmarks in semantic tasks such as image classification, semantic segmentation and human pose estimation. Additionally, recent works such as FlowNet [7], Deep Semantic Matching [1] and Eigen *et al.*'s Multi-Scale Deep Network [5] present promising results for dense geometric computer vision tasks like optical flow and depth estimation. Even robotic tasks like visual odometry are being tackled with convolutional neural networks [4].

In this paper, we show that the entire homography estimation problem can be solved by a deep convolutional neural network (See Figure 1). Our contributions are as follows: we present a new VGG-style [17] network for the homography estimation task. We show how to use the 4-point parameterization [2] to get a well-behaved deep estimation problem. Because deep networks require a lot of data to be trained from scratch, we share our recipe for creating a seemingly infinite dataset of (I_A, I_B, H^{AB}) training triplets from an existing dataset of real images like the MS-COCO dataset. We present an additional formulation of the homography estimation problem as classification, which produces a distribution over homographies and can be used to determine the confidence of an estimated homography.

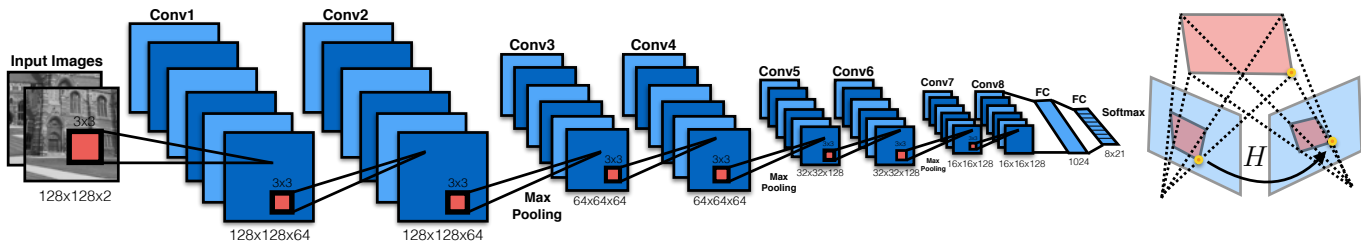


Fig. 1: **Deep Image Homography Estimation.** HomographyNet is a Deep Convolutional Neural Network which directly produces the Homography relating two images. Our method does not require separate corner detection and homography estimation steps and all parameters are trained in an end-to-end fashion using a large dataset of labeled images.

II. THE 4-POINT HOMOGRAPHY PARAMETERIZATION

The simplest way to parameterize a homography is with a 3×3 matrix and a fixed scale. The homography maps $[u, v]$, the pixels in the left image, to $[u', v']$, the pixels in the right image, and is defined up to scale (see Equation 1).

$$\begin{pmatrix} u' \\ v' \\ 1 \end{pmatrix} \sim \begin{pmatrix} H_{11} & H_{12} & H_{13} \\ H_{21} & H_{22} & H_{23} \\ H_{31} & H_{32} & H_{33} \end{pmatrix} \begin{pmatrix} u \\ v \\ 1 \end{pmatrix} \quad (1)$$

However, if we unroll the 8 (or 9) parameters of the homography into a single vector, we'll quickly realize that we are mixing both rotational and translational terms. For example, the submatrix $[H_{11} \ H_{12}; \ H_{21} \ H_{22}]$, represents the rotational terms in the homography, while the vector $[H_{13} \ H_{23}]$ is the translational offset. Balancing the rotational and translational terms as part of an optimization problem is difficult.

We found that an alternate parameterization, one based on a single kind of location variable, namely the corner location, is more suitable for our deep homography estimation task. The 4-point parameterization has been used in traditional homography estimation methods [2], and we use it in our modern deep manifestation of the homography estimation problem (See Figure 2). Letting $\Delta u_1 = u'_1 - u_1$ be the u-offset for the first corner, the 4-point parameterization represents a homography as follows:

$$H_{4point} = \begin{pmatrix} \Delta u_1 & \Delta v_1 \\ \Delta u_2 & \Delta v_2 \\ \Delta u_3 & \Delta v_3 \\ \Delta u_4 & \Delta v_4 \end{pmatrix} \quad (2)$$

Equivalently to the matrix formulation of the homography, the 4-point parameterization uses eight numbers. Once the displacement of the four corners is known, one can easily convert H_{4point} to H_{matrix} . This can be accomplished in a number of ways, for example one can use the normalized Direct Linear Transform (DLT) algorithm [9], or the function `getPerspectiveTransform()` in OpenCV.

III. DATA GENERATION FOR HOMOGRAPHY ESTIMATION

Training deep convolutional networks from scratch requires a large amount of data. To meet this requirement, we generate a nearly unlimited number of labeled training examples by applying random projective transformations to a large dataset

of natural images¹. The process is illustrated in Figure 3 and described below.

To generate a single training example, we first randomly crop a square patch from the larger image I at position p (we avoid the borders to prevent bordering artifacts later in the data generation pipeline). This random crop is I_p . Then, the four corners of Patch A are randomly perturbed by values within the range $[-\rho, \rho]$. The four correspondences define a homography H^{AB} . Then, the inverse of this homography $H^{BA} = (H^{AB})^{-1}$ is applied to the large image to produce image I' . A second patch I'_p is cropped from I' at position p . The two grayscale patches, I_p and I'_p are then stacked channel-wise to create the 2-channel image which is fed directly into our ConvNet. The 4-point parameterization of H^{AB} is then used as the associated ground-truth training label.

Managing the training image generation pipeline gives us full control over the kinds of visual effects we want to model. For example, to make our method more robust to motion blur, we can apply such blurs to the image in our training set. If we want the method to be robust to occlusions, we can insert random occluding shapes into our training images. We experimented with in-painting random occluding rectangles into our training images, as a simple mechanism to simulate real occlusions.

¹In our experiments, we used cropped MS-COCO [13] images, although any large-enough dataset could be used for training

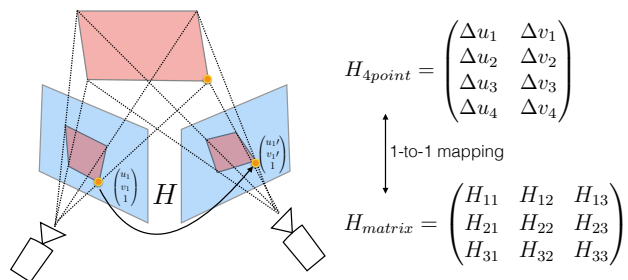


Fig. 2: **4-point parameterization.** We use the 4-point parameterization of the homography. There exists a 1-to-1 mapping between the 8-dof "corner offset" matrix and the representation of the homography as a 3×3 matrix.

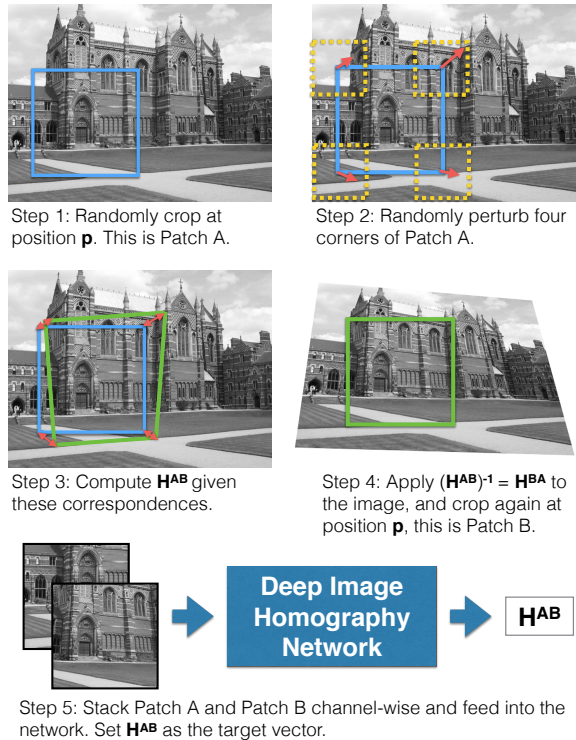


Fig. 3: **Training Data Generation.** The process for creating a single training example is detailed. See Section III for more information.

IV. CONVNET MODELS

Our networks use 3x3 convolutional blocks with Batch-Norm [10] and ReLUs, and are architecturally similar to Oxfords VGG Net [17] (see Figure 1). Both networks take as input a two-channel grayscale image sized $128 \times 128 \times 2$. In other words, the two input images, which are related by a homography, are stacked channel-wise and fed into the network. We use 8 convolutional layers with a max pooling layer (2x2, stride 2) after every two convolutions. The 8 convolutional layers have the following number of filters per layer: 64, 64, 64, 64, 128, 128, 128, 128. The convolutional layers are followed by two fully connected layers. The first fully connected layer has 1024 units. Dropout with a probability of 0.5 is applied after the final convolutional layer and the first fully-connected layer. Our two networks share the same architecture up to the last layer, where the first network produces real-valued outputs and the second network produces discrete quantities (see Figure 4).

The **regression network** directly produces 8 real-valued numbers and uses the Euclidean (L2) loss as the final layer during training. The advantage of this formulation is the simplicity; however, without producing any kind of confidence value for the prediction, such a direct approach could be prohibitive in certain applications.

The **classification network** uses a quantization scheme, has a softmax at the last layer, and we use the cross entropy loss

function during training. While quantization means that there is some inherent quantization error, the network is able to produce a confidence for each of the corners produced by the method. We chose to use 21 quantization bins for each of the 8 output dimensions, which results in a final layer with 168 output neurons. Figure 6 is a visualization of the corner confidences produced by our method — notice how the confidence is not equal for all corners.

V. EXPERIMENTS

We train both of our networks for about 8 hours on a single Titan X GPU, using stochastic gradient descent (SGD) with momentum of 0.9. We use a base learning rate of 0.005 and decrease the learning rate by a factor of 10 after every 30,000 iterations. The networks are trained for 90,000 total iterations using a batch size of 64. We use Caffe [11], a popular open-source deep learning package, for all experiments.

To create the training data, we use the MS-COCO Training Set. All images are resized to 320×240 and converted to grayscale. We then generate 500,000 pairs of image patches sized 128×128 related by a homography using the method described in Section III. We choose $\rho = 32$, which means that each corner of the 128×128 grayscale image can be perturbed by a maximum of one quarter of the total image edge size. We avoid larger random perturbations to avoid extreme transformations. We did not use any form of pre-training; the weights of the networks were initialized to random values and trained from scratch. We use the MS-COCO validation set to monitor overfitting, of which we found very little.

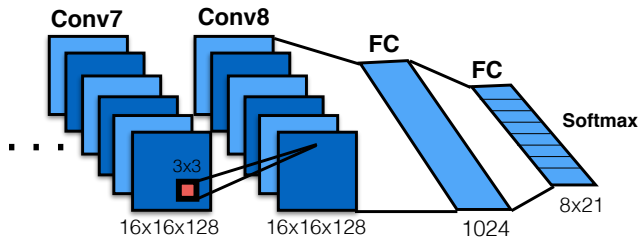
To our knowledge there are no large, publicly available homography estimation test sets, thus we evaluate our homography estimation approach on our own Warped MS-COCO 14 Test Set. To create this test set, we randomly chose 5000 images from the test set and resized each image to grayscale 640×480 , and generate a pairs of image patches sized 256×256^2 and corresponding ground truth homography, using the approach described in Figure 3 with $\rho = 64$.

We compare the Classification and Regression variants of the HomographyNet with two baselines. The first baseline is a classical ORB [15] descriptor + RANSAC + `getPerspectiveTransform()` OpenCV Homography computation. We use the default OpenCV parameters in the traditional homography estimator. This estimates ORB features at multiple scales and uses the top 25 scoring matches as input to the RANSAC estimator. In scenarios where too few ORB features are computed, the ORB+RANSAC approach outputs an identity estimate. In scenarios where the ORB+RANSAC's estimate is too extreme, the 4-point homography estimate is clipped at $[-64, 64]$. The second baseline uses a 3x3 identity matrix for every pair of images in the test set.

Since the HomographyNets expect a fixed sized $128 \times 128 \times 2$ input, the image pairs from the Warped MS-COCO 14 Test Set are resized from $256 \times 256 \times 2$ to $128 \times 128 \times 2$ before being passed

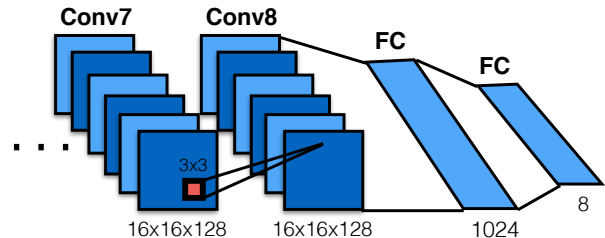
²We found that very few ORB features were detected when the patches were sized 128×128 , while the HomographyNets had no issues working at the smaller scale.

Classification HomographyNet



$$\text{Loss: Cross-Entropy} - \sum_x p(x) \log q(x)$$

Regression HomographyNet



$$\text{Loss: Euclidean (L2)} \quad \frac{1}{2} \|p(x) - q(x)\|^2$$

Fig. 4: **Classification HomographyNet vs Regression HomographyNet.** Our VGG-like Network has 8 convolutional layers and two fully connected layers. The final layer is 8x21 for the classification network and 8x1 for the regression network. The 8x21 output can be interpreted as four 21x21 corner distributions. See Section IV for full ConvNet details.

through the network. The 4-point parameterized homography output by the network is then multiplied by a factor of two to account for this. When evaluating the Classification HomographyNet, the corner displacement with the highest confidence is chosen.

The results are reported in Figure 5. We report the Mean Average Corner Error for each approach. To measure this metric, one first computes the L2 distance between the ground truth corner position and the estimated corner position. The error is averaged over the four corners of the image, and the mean is computed over the entire test set. While the regression network performs the best, the classification network can produce confidences and thus a meaningful way to visually debug the results. In certain applications, it may be critical to have this measure of certainty.

We visualize homography estimations in Figure 7. The blue squares in column 1 are mapped to a blue quadrilateral in column 2 by a random homography generated from the process described in Section III. The green quadrilateral is the estimated homography. The more closely the blue and green quadrilateral align, the better. The red lines show the top scoring matches of ORB features across the image patches. A similar visualization is shown in columns 3 and 4, except the Deep Homography Estimator is used.

VI. APPLICATIONS

Our Deep Homography Estimation system enables a variety of interesting applications. Firstly, our system is fast. It runs at over 300fps with a batch size of one (i.e. real-time inference mode) on an NVIDIA Titan X GPU, which enables a host of applications that are simply not possible with a slower system. The recent emergence of specialized embedded hardware for deep networks will enable applications on many embedded systems or platforms with limited computational power which cannot afford an expensive and power-hungry desktop GPU. These embedded systems are capable of running much larger networks such as AlexNet [12] in real-time, and should have no problem running the relatively light-weight HomographyNets.

Secondly, by formulating homography estimation as a machine learning problem, one can build application-specific homography estimation engines. For example, a robot that navigates an indoor factory floor using planar SLAM via homography estimation could be trained solely with images captured from the robot’s image sensor of the indoor factory. While it is possible to optimize a feature detector such as ORB to work in specific environments, it is not straightforward. Environment and sensor-specific noise, motion blur, and occlusions which might restrict the ability of a homography estimation algorithm can be tackled in a similar fashion using a ConvNet. Other classical computer vision tasks such as image mosaicing (as in [19]) and markerless camera tracking systems

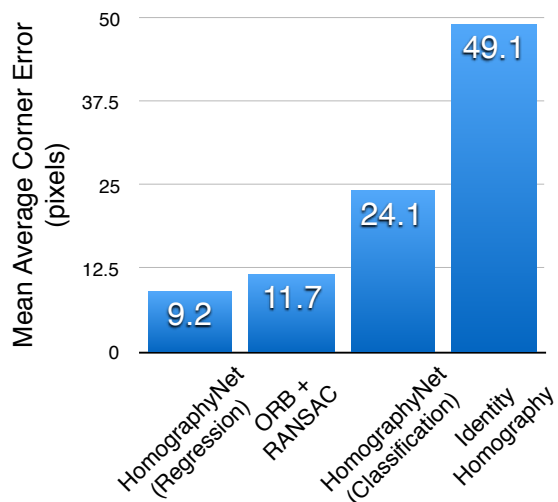


Fig. 5: **Homography Estimation Comparison on Warped MS-COCO 14 Test Set.** The mean average corner error is computed for various approaches on the Warped MS-COCO 14 Test Set. The HomographyNet with the regression head performs the best. The far right bar shows the error computed if the identity transformation is estimated for each test pair.

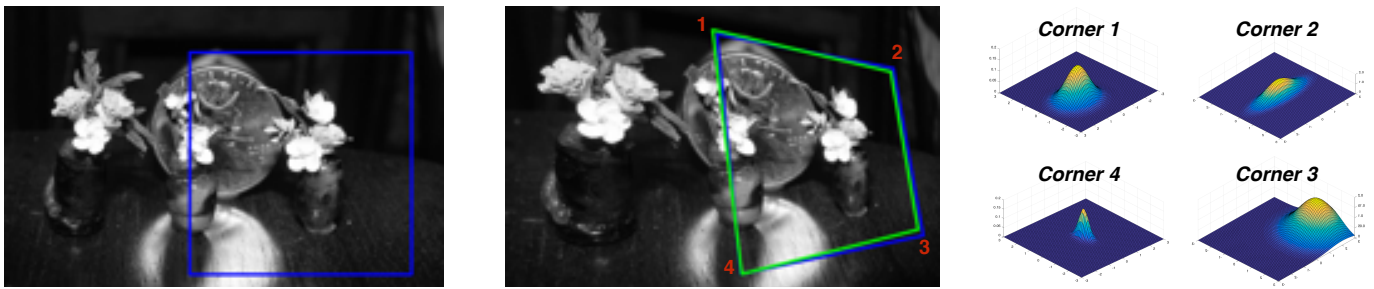


Fig. 6: **Corner Confidences Measure.** Our Classification HomographyNet produces a score for each potential 2D displacement of each corner. Each corner's 2D grid of scores can be interpreted as a distribution.

for augmented reality (as in [16]) could also benefit from HomographyNets trained on image pair examples created from the target system's sensors and environment.

VII. CONCLUSION

In this paper we asked if one of the most essential computer vision estimation tasks, namely homography estimation, could be cast as a learning problem. We presented two Convolutional Neural Network architectures that are able to perform well on this task. Our end-to-end training pipeline contains two additional insights: using a 4-point corner parameterization of homographies, which makes the parameterizations coordinates operate on the same scale, and using a large dataset of real image to synthetically create an seemingly unlimited-sized training set for homography estimation. We hope that more geometric problems in vision will be tackled using learning paradigms.

REFERENCES

- [1] M. Bai, W. Luo, K. Kundu, and R. Urtasun. Deep Semantic Matching for Optical Flow. *CoRR*, abs/1604.01827, April 2016.
- [2] Simon Baker, Ankur Datta, and Takeo Kanade. Parameterizing homographies. Technical Report CMU-RI-TR-06-11, Robotics Institute, Pittsburgh, PA, March 2006.
- [3] Matthew Brown and David G Lowe. Automatic panoramic image stitching using invariant features. *International journal of computer vision*, 74(1):59–73, 2007.
- [4] G. Costante, M. Mancini, P. Valigi, and T. A. Ciarfuglia. Exploring representation learning with cnns for frame to frame ego-motion estimation. *ICRA*, 2016.
- [5] David Eigen, Christian Puhrsch, and Rob Fergus. Depth map prediction from a single image using a multi-scale deep network. *CoRR*, abs/1406.2283, 2014.
- [6] J. Engel, T. Schöps, and D. Cremers. LSD-SLAM: Large-scale direct monocular SLAM. 2014.
- [7] Philipp Fischer, Alexey Dosovitskiy, Eddy Ilg, Philip Häusser, Caner Hazirbas, Vladimir Golkov, Patrick van der Smagt, Daniel Cremers, and Thomas Brox. FlowNet: Learning optical flow with convolutional networks. *ICCV*, 2015.
- [8] A. P. Gee, D. Chekhlov, A. Calway, and W. Mayol-Cuevas. Discovering higher level structure in visual slam. *IEEE Transactions on Robotics*, 2008.
- [9] R. I. Hartley and A. Zisserman. *Multiple View Geometry in Computer Vision*. Cambridge University Press, ISBN: 0521540518, second edition, 2004.
- [10] Sergey Ioffe and Christian Szegedy. Batch normalization: Accelerating deep network training by reducing internal covariate shift. *CoRR*, abs/1502.03167, 2015.
- [11] Y. Jia, E. Shelhamer, J. Donahue, S. Karayev, J. Long, R. Girshick, S. Guadarrama, and T. Darrell. Caffe: Convolutional architecture for fast feature embedding. *arXiv preprint arXiv:1408.5093*, 2014.
- [12] Alex Krizhevsky, Ilya Sutskever, and Geoffrey E. Hinton. Imagenet classification with deep convolutional neural networks. In *NIPS*. 2012.
- [13] Tsung-Yi Lin, Michael Maire, Serge Belongie, James Hays, Pietro Perona, Deva Ramanan, Piotr Dollr, and C. Lawrence Zitnick. Microsoft coco: Common objects in context. In *ECCV*, 2014.
- [14] R. Mur-Artal, J. M. M. Montiel, and J. D. Tardós. Orb-slam: A versatile and accurate monocular slam system. *IEEE Transactions on Robotics*, 2015.
- [15] Ethan Rublee, Vincent Rabaud, Kurt Konolige, and Gary Bradski. Orb: An efficient alternative to sift or surf. In *ICCV*, 2011.
- [16] G. Simon, A. Fitzgibbon, and A. Zisserman. Markerless tracking using planar structures in the scene. In *Proc. International Symposium on Augmented Reality*, pages 120–128, October 2000.
- [17] K. Simonyan and A. Zisserman. Very deep convolutional networks for large-scale image recognition. *CoRR*, abs/1409.1556, 2014.
- [18] Paul Smith, Ian Reid, and Andrew Davison. Real-time monocular SLAM with straight lines. In *Proc. British Machine Vision Conference*, 2006.
- [19] Richard Szeliski. Video mosaics for virtual environments. *IEEE Computer Graphics and Applications*, 1996.
- [20] Zhengyou Zhang. A flexible new technique for camera calibration. *PAMI*, 22(11):1330–1334, 2000.

Traditional Homography Estimation

Deep Image Homography Estimation

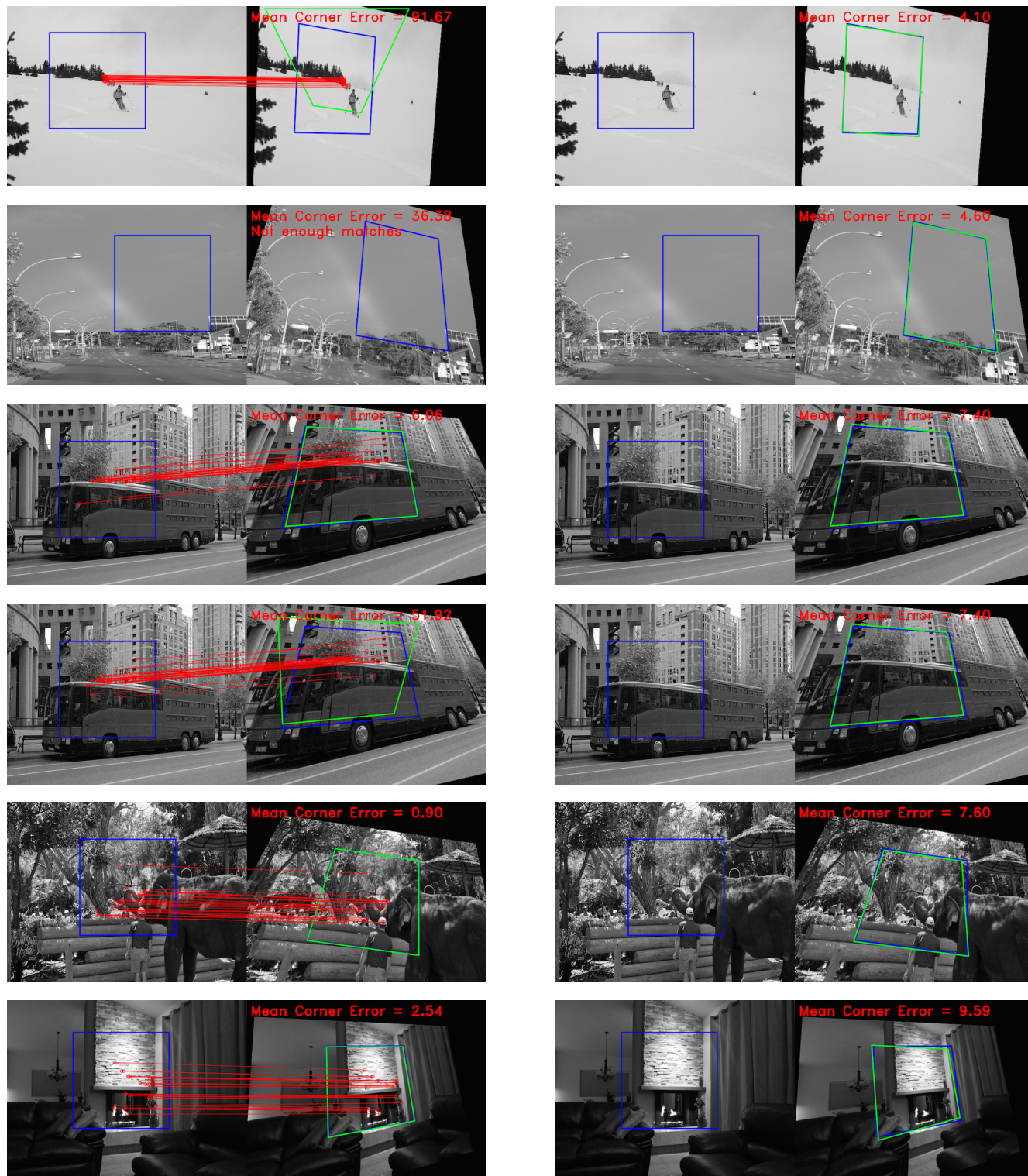


Fig. 7: Traditional Homography Estimation vs Deep Image Homography Estimation. In each of the 12 examples, blue depicts the ground truth region. The left column shows the output of ORB-based Homography Estimation, the matched features in red, and the resulting mapping in green of the cropping. The right column shows the output of the HomographyNet (regression head) in green. Rows 1-2: The ORB features either concentrate on small regions or cannot detect enough features and perform poorly relative to the HomographyNet, which is unaffected by these phenomena. Row 3: Both methods give reasonably good homography estimates. Row 4: A small amount of Gaussian noise is added to the image pair in row 3, deteriorating the results produced by the traditional method, while our method is unaffected by the distortions. Rows 5-6: The traditional approach extracts well-distributed ORB features, and also outperforms the deep method.